Microstructure and property evolution of diamond-like carbon films co-doped by Al and Ti with different ratios

Yong Zhou[a,b], Peng Guo[a], Lili Sun[a], Linlin Liu[a], Xiaowei Xu[a], Wenxian Li[b], Xiaowei Li[a,c,*], Kwang-Ryeol Lee[c], Aiying Wang[a,d,**]

[a] Key Laboratory of Marine Materials and Related Technologies, Zhejiang Key Laboratory of Marine Materials and Protective Technologies, Ningbo Institute of Materials Technology and Engineering, Chinese Academy of Sciences, Ningbo 315201, China
[b] School of Materials Science and Engineering, Shanghai University, Shanghai 200444, China
[c] Computational Science Center, Korea Institute of Science and Technology, Seoul 136-791, Republic of Korea
[d] Center of Materials Science and Optoelectronics Engineering, University of Chinese Academy of Sciences, Beijing 100049, China

ARTICLE INFO

ABSTRACT

Diamond-like carbon (DLC) films with weak carbide metal Al and carbide metal Ti co-doping (Al/Ti-DLC) were prepared by a hybrid ion beam deposition system. The atomic ratios of doped Al to Ti were tailored via designing the special Al/Ti combined sputtering target. The composition, microstructure, roughness, residual stress, hardness, toughness, and tribological behaviors of the deposited films were systematically evaluated to explore the dependence of structural properties on Al/Ti ratios. Results indicated that the high-throughput preparation of DLC films with different Al/Ti atomic ratios was achieved by tailoring the sputtering target and process parameters without the difference in both the film thickness and total Al/Ti content. With the Al/Ti ratios in the films decreased from 8.8 to 3.0, the residual stress, hardness, and toughness of Al/Ti-DLC films increased obviously, originating from the increased fraction of titanium carbide and the reduced Al content. However, the coefficient of friction and wear rate with decreasing the Al/Ti ratio were obviously improved, which was related with the transformation of underlying friction mechanism from the sliding interface graphitization to dangling bond-passivation. The present results not only suggest a high-throughput method to fabricate co-doped DLC films, but also promote the scientific understanding and engineering application of DLC films with high performance.

1. Introduction

Diamond-like carbon (DLC) film is a metastable form of amorphous carbon, which has a mixture of diamond structure (sp^3C hybridization) and a graphite structure (sp^2C hybridization) [1]. This special structure endows DLC film with superior physicochemical properties including excellent mechanical and tribological properties. Especially, due to their eco-friendly fabrication process, DLC films are attracting more and more interest for engineering and technical applications [2–5], and many third elements, such as Ti, Cr, W, N, F, etc., also have been widely doped into the amorphous carbon network in order to further adjust the structural properties and overcome the intrinsic disadvantages of DLC films [6–11].

As well known that the structural properties of metal doped DLC films are closely related with the type, content and chemical state of doped metal element. For example, when the weak-carbide-formers (WCF), such as Al [12] and Ag [13], are introduced into carbon networks, they are inclined to form the soft and ductile clusters, rather than bond with carbon atoms, thus improving the toughness and releasing the high intrinsic stress by means of plastic deformation, but the corresponding hardness of film is also deteriorated drastically. Instead, the strong-carbide-formers (SCF), such as Ti [14], Cr [15], etc., are covalently bonded with carbon to form the hard carbide crystallites, embedding in the amorphous structure and resulting in the increased residual stress, although the hardness of the films can be improved obviously. Until now, it is still of big challenge to tailor a DLC film with an excellent combined property by the single addition of WCF or SCF atoms.

Many experimental and calculation efforts indicated that the co-doping of SCF and WCF metals was confirmed to be an effective approach for further modulating the structure of DLC films and also exhibited that the co-doped metal content played a critical role in the combined properties [16–20]. The excess SCF metal elements can cause the increased fraction of metal carbide and deteriorate the tribological performance. In order to obtain films with good tribological properties, low intrinsic stress, and high hardness, it is required to accurately control the quantity, morphology, and distribution of nanocrystalline carbides and optimize the content of doped elements. For example, Mandal et al. [21] found that when the Ti and W contents were 0.3 at.% and 2.6 at.%, respectively, the DLC film possessed the lowest coefficient of friction (COF) and wear rate. However, the evolution of microstructure, mechanical, and tribological properties with co-doped metal content, especially its dependence on the atomic ratios between the co-doped metals, is not fully understood yet due to the technical challenge, which is the complicated preparation of co-doped DLC films with different ratios normally requiring multiple groups of samples and thus leading to the various uncertainties or difference in cavity environment, film thickness, and total content of co-doped. Exploring the relation between the ratio of co-doped metals and structural properties is still required for tailoring the high-performance DLC films.

In previous works [22–25], the Al/Ti co-doped DLC (Al/Ti-DLC) films have been prepared using hybrid ion beam (HIB) system, and the structural property evolution with Al/Ti contents and various process parameters (sputtering current, gas source, and bias voltage) has also been systematically explored. Hence, in the present study, the HIB system was also adopted to fabricate the Al/Ti-DLC films. In particular, based on the high-throughput concept, we successfully realized the single-step preparation of multiple DLC films with different Al/Ti ratios by the special design of sputtering target materials. The Al/Ti ratio-induced evolutions of structure and properties of films were mainly focused on to disclose the underlying structure-property relationship. It indicated that the residual intrinsic stress, mechanical and tribological behaviors were closely sensitive to the Al/Ti ratios and corresponding evolution in structure.

2. Experimental methods

2.1. Preparation of Al/Ti-DLC films

Al/Ti-DLC films were prepared by a HIB system consisting of a DC magnetron sputtering with Al (99.99% purity)/Ti (99.99% purity) combined target and a linear anode-layer ion source (ALIS) with C_2H_2 gas, as shown in Fig. 1a. The schematic diagram for designed Al/Ti combined target and substrate placement during deposition process was given in Fig. 1b to modulate the Al/Ti ratios. Si (100) wafers and 316 L were selected as substrate; a thin silicon substrate with thickness of $250 \pm 5\,\mu m$ was also adopted in order to accurately evaluate the residual internal stress.

The distances between the substrates and ALIS or Al/Ti target were 17 cm, respectively (Fig. 1a). Before the deposition, the chamber vacuum was exhausted to a value of about 2.0×10^{-5} Torr, and then Ar ion was applied to etch the substrates for 20 min at −100 V in order to clear the surface contaminations; the Al/Ti combined target was sputtered via Ar for 5 min. During the deposition process, the C_2H_2 as hydrocarbon gas was imported into the ALIS for carbon deposition, while the inert gas, Ar, was provided to the magnetron sputtering for Al/Ti co-doping; the total deposition time was 2 h and the substrate holder rotated in a different direction every 15 min. Table 1 gave the main process parameters used, and others could be found in previous study [23].

2.2. Composition and microstructure characterization

Surface profilometer (Alpha-step IQ, US) with a shadow mask between the bare Si wafers and films was used to measure the film thickness. X-ray photoelectron spectroscopy (XPS, Thermo Scientific ESCALAB 250) was only adopted to assess the chemical bonding of co-doped metals and the composition of deposited films and wear scars due to the lack of universal fitting standard for XPS C 1s spectra [26–28], such as position and full width at half maximum (FWHM) of both sp^2-C and sp^3-C peaks; before measure, Ar^+ was employed to etch the film surface for clean surface. The atomic bond structure of carbon was detected by means of Raman spectrometer (Renishaw inVia Reflex, wavelength-532 nm). The roughness and surface topography of deposited film were characterized using a tapping mode atomic force microscope by a scanning probe microscope (Veeco Dimension 3100 V, SPM). The surface morphologies of wear scars on the contact ball and wear tracks on the film were estimated, respectively, through scanning electron microscopy (SEM); in addition, the compositions of the film, wear track, and wear scar, were quantified by the energy dispersive X-ray spectroscopy (EDS), respectively. The evolution of microstructure with Al/Ti ratios was characterized by high-resolution transmission electron microscopy (HR-TEM, Tecnai F20, US).

2.3. Mechanical and tribological property tests

Nanoindenter (MTS-G200) was performed to measure the hardness and elastic modulus; six replicate indentations were carried out for each film, the maximal indentation depth was 500 nm, and the values in 1/10 film thickness were employed for eliminating the substrate-induced influence on results. In order to evaluate the toughness of the film, Vickers hardness tester was conducted to measure the indentation diameters, which worked under 5 N. Residual stress tester (JLCST022, J &L Tech) was provided to estimate the residual internal stress according to the Stoney equation.

The tribological properties of the deposited films were evaluated using the ball-on-disk reciprocating tribometer (UMT-3), which worked at atmosphere environment. A grinding 6-mm-diameter Si_3N_4 ball
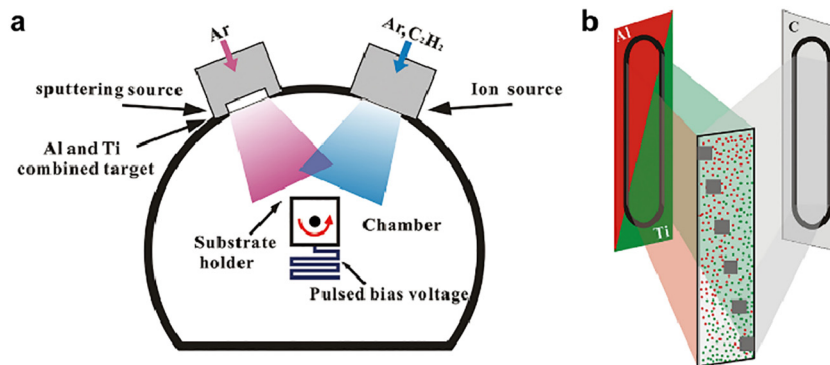

Fig. 1. (a) Schematic diagram of HIB deposition system. (b) Designed Al/Ti combined target and substrate placement during the deposition process.

Table 1
Deposition parameters for the Al/Ti-DLC films.

Sputtering current (A)	Ar flow rate (sccm)	LIS working current (A)	LIS working voltage (V)	C_2H_2 flow rate (sccm)	Bias voltage (V)	Working pressure (Pa)
2.5	70	0.5	1100 ± 50	10	−50	0.6

(HRC75) was selected as the mating material. During the friction process, the sliding velocity, applied normal load, and reciprocating frequency were 5 cm/s, 15 N, and 5 Hz, respectively; the wear track length was 5 mm, and the sliding time was 1800 s. After tests, the wear rate for each sample was counted based on Archard equation:

$$W = \frac{V}{N * L} \tag{1}$$

where L and N are total sliding distance and normal load separately; W and V are wear rate and volume loss, respectively. Here, the V was calculated by the multiplying operation of the length and the cross-sectional profiles of wear tracks.

3. Results and discussion

3.1. Thickness and composition

Fig. 2 shows the composition and thickness of the Al/Ti-DLC films at different locations. First, the total content of both Ti and Al atoms is kept at about 8.15 ± 0.99 at.% for each case, which is comparable to the previous study [25]. However, it can be observed that from the top to bottom positions in Fig. 1b, the Ti content increases from 0.91 to 1.83 at.% following the reduction of Al content from 7.98 to 5.34 at.%, which corresponds to the Al/Ti ratio ranged from 8.8 to 3.0 (Fig. 2a). Furthermore, the similar thickness of Al/Ti-DLC film, which is about 1.38 ± 0.17 μm (Fig. 2b), is also obtained for each case. This indicates that by the special design of Al/Ti combined composite target, the high-throughput fabrication of Al/Ti-DLC films with different Al/Ti ratios is successfully achieved at one time, which have constant values of thickness and total Al/Ti content, excluding the effect of total content and thickness on the film performance. In addition, it should be mentioned that during the deposition process, the moisture adsorbed by the chamber wall is evaporated out, resulting in the existence of oxygen content in the deposited film.

3.2. Chemical bond and microstructure

XPS spectra with different Al/Ti ratios, including C 1s, Ti 2p, and Al 2p, are illustrated in Fig. 3. In each C 1s spectrum (Fig. 3a), there is a major peak presented at 284.6 eV, attributing to the amorphous carbon

structure, and the peak intensity has no obvious difference for each case due to the same C content in the film. For each sample, the C 1s spectrum can be divided into four peaks (Fig. 3d), which correspond to the sp^3-C bond at 285.2 eV, sp^2-C bond at 284.4 eV, C−O bond at 287 eV, and Ti−C bond at 282.7 eV [29], respectively. For each Al 2p spectrum (Fig. 3b), Fig. 3e shows that two peaks are identified; the peak at 74 eV represents Al−O bond, while the other at 75.3 eV is related with Al−O−H bond [30], implying that the Al is presented mainly as oxided rather than metallic state in the carbon matrix due to the inevitable oxygen during the deposition process. However, the Ti 2p spectrum (Fig. 3c) can be deconvoluted into four components (Fig. 3f), in which a pair of peaks, located at 455.6 eV and 461.6 eV separately, are corresponding to the Ti−C bond, and the other pair of peaks (458 eV and 463.7 eV) are assigned to the Ti−O bond, suggesting that Ti exists as a hard phase of titanium carbide and TiO_x in the carbon matrix.

The microstructure and phase structure of Al/Ti-DLC film with different Al/Ti ratios are further characterized by HR-TEM. Fig. 4 gives the cross-sectional HR-TEM micrographs of the Al/Ti-DLC films with different Al/Ti ratios of 8.8 ($Al_{7.98}Ti_{0.91}$-DLC), 5.0 ($Al_{7.48}Ti_{1.51}$-DLC) and 3.0 ($Al_{5.43}Ti_{1.83}$-DLC), respectively, in which the insets are the corresponding selected area electron diffraction (SAED) patterns. For the film with Al/Ti ratio of 8.8 (Fig. 4a), a broad and diffuse halo is observed in the SAED pattern, which is a typical characteristic of amorphous carbon structure; although a Ti−C peak exists in the C1s spectra (Fig. 3d), there is no lattice fringes found from the TEM micrograph, which results from the low fraction and poor crystallinity of formed titanium carbide in the film. With the Al/Ti ratio decreased to 5.0 (Fig. 4b) and 3.0 (Fig. 4c), respectively, the nanocrystalline TiC phase can be clearly distinguished in the film, which is also accompanied by the increased size and amount of TiC nanocrystals due to the increased Ti content. This is in consistence with the analysis of XPS spectra (Fig. 3).

Fig. 5a displays the Raman spectra of Al/Ti-DLC films with different Al/Ti ratios. The spectra shows the typical feature of intrinsic DLC film for each case, that is the appearance of an asymmetric scattering curve. The fitted result of Raman using double Gaussian function is shown in Fig. 5a. Note that each Raman spectrum consists of two peaks; the peak around 1580 cm^{-1}, named G peak, attributes to the bond stretching of sp^2-C atoms including both chains and aromatic rings, and the other
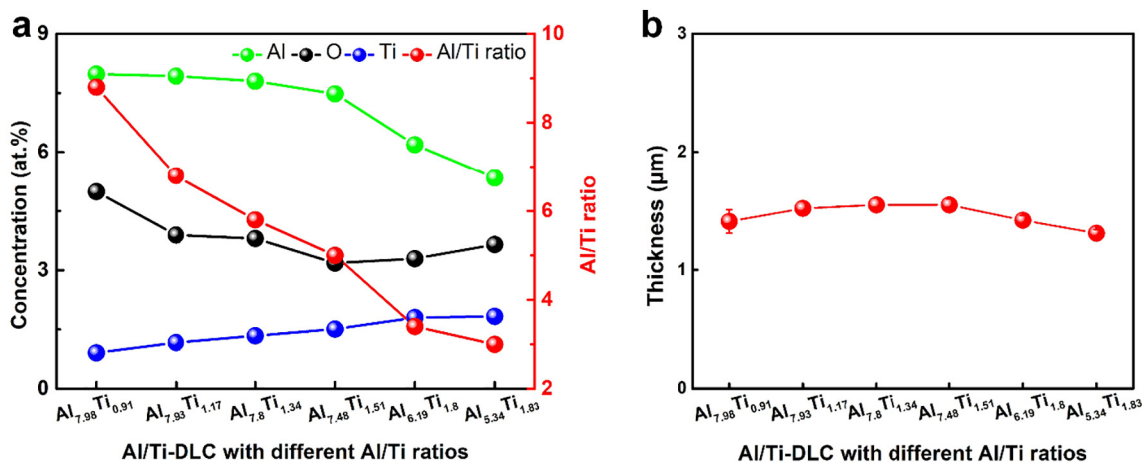

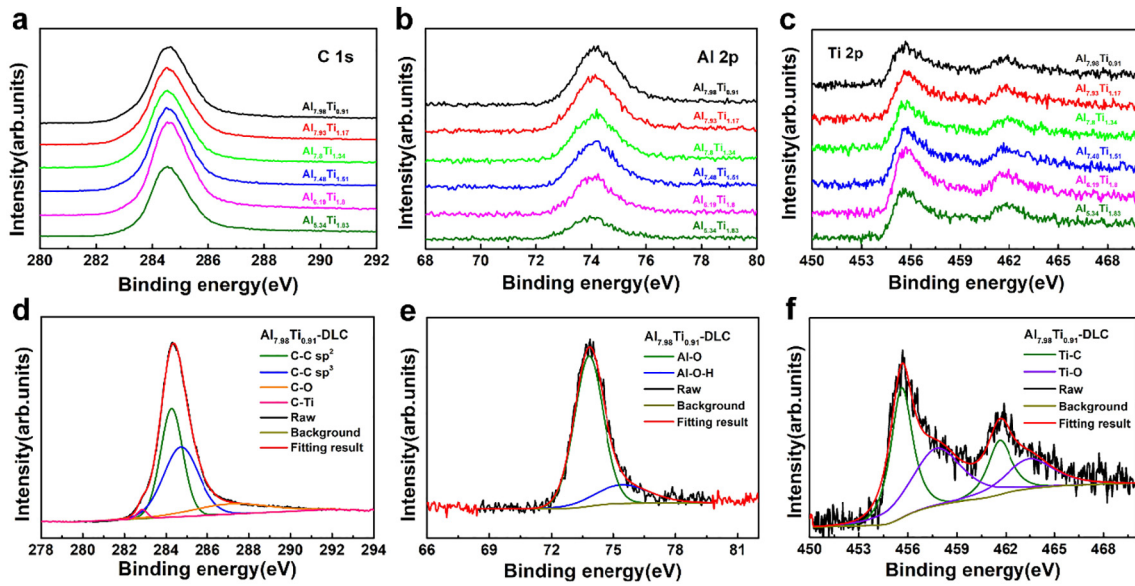**Fig. 2.** (a) Composition and (b) thickness of the deposited Al/Ti-DLC films.

Fig. 3. XPS results including (a) C 1s, (b) Al 2p, and (c) Ti 2p spectra of Al/Ti-DLC films with different Al/Ti ratios, and fitting results of (d) C 1 s, (e) Al 2p, (f) Ti 2p XPS peak for the $Al_{7.98}Ti_{0.91}$-DLC film.

around 1350 cm^{-1}, named as D peak, is only from the breathing modes of sp^2-C atoms in aromatic rings [31]. Fig. 5b further gives the intensity ratio of D peak to G peak (I_D/I_G), G peak position, and FWHM of G peak (G_{FWHM}). Normally, the I_D/I_G ratio and G peak position can reflect the variation of sp^2/sp^3 ratio in the amorphous carbon films; the increase of both I_D/I_G ratio and G peak position suggests high sp^2/sp^3 ratio [32]; the G_{FWHM} is correlated with the degree of disorder in amorphous structure. Results in Fig. 5b reveals that as the Al/Ti ratio decreases, the I_D/I_G of Al/Ti-DLC films slowly increases and the G peak position shifts slightly to higher position. Hence, it suggested that reducing the Al/Ti ratio from 8.8 to 3.0 causes the increase of sp^2 content. The G_{FWHM} also increases slightly with the decrease of Al/Ti ratio, indicating the increased bond length of sp^2-C in the film, which induces the disorder of the carbon bond structure [33]. The Ti atoms easily bond with C to reduce the suspended bond in the film and thus reduce the content of sp^3 in the film, leading to the formation of nanocarbide in Al/Ti-DLC films. In addition, previous ab initio calculation [34] also confirmed that Ti atoms could effectively catalyze the sp^3-to-sp^2 transformation in amorphous carbon structure at low temperature, which also contributes to the increased sp^2 content in the Al/Ti-DLC films with Al/Ti ratios ranged from 8.8 to 3.0.

3.3. Residual stress and mechanical property

The changes of residual stress and mechanical property of Al/Ti-DLC films with Al/Ti ratios are illustrated in Fig. 6a. Note that with decreasing the Al/Ti ratio from 8.8 to 3.0, the hardness increases from 13.8 ± 1.7 to 19.6 ± 0.7 GPa, which is consistent with the change of

elastic modulus. This attributes to the relative change of Al and Ti contents in the film. Combined with the contribution of reduced Al content to hardness, the increased Ti content (Fig. 2) leads to the generation and increased fraction of titanium carbide nanocrystallites (Fig. 4), which can make up the destruction of amorphous carbon structures and thus improve the hardness of the films. For the residual compressive stress, it also exhibits the similar dependence on Al/Ti ratio to hardness, which increases from 0.5 ± 0.01 to 1.0 ± 0.09 GPa gradually, but these values are still much lower than that in the intrinsic DLC films [25]. This increased residual compressive stress is mainly dominated by the increase of titanium carbide in the do-doped films [35] because the Al presents as oxidation state, which cannot play a critical site to relax the distorted bond structure effectively [25].

Furthermore, Fig. 6b shows variation of both the H/E and H^3/E^2 ratios with Al/Ti ratio, in which the fracture toughness is related with the H/E value, while the resistance to plastic deformation can be represented by H^3/E^2 value. The H/E ratio with Al/Ti ratio has small change, but the H^3/E^2 ratio increases significantly, implying the improved toughness of Al/Ti-DLC films. Fig. 6c further gives the SEM images of radial cracks at the Vickers indentation for each case to qualitatively analyze the toughness of Al/Ti-DLC film. Note that as the Al/Ti ratio decreases from 8.8 to 3.0, the indentation radial crack length of Al/Ti-DLC film decreases. The fracture toughness value, K_{IC}, for each film is calculated using the following equation:

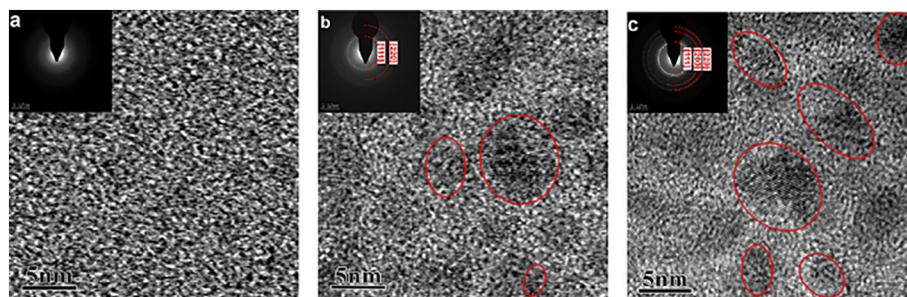$$K_{IC} = b\left(\frac{E}{H}\right)^{1/2}\left(\frac{P}{c^{3/2}}\right)$$

(2)

Fig. 4. The HR-TEM micrographs and corresponding SAED patterns of (a) $Al_{7.98}Ti_{0.91}$-DLC, (b) $Al_{7.48}Ti_{1.51}$-DLC, and (c) $Al_{5.43}Ti_{1.83}$-DLC films, respectively.
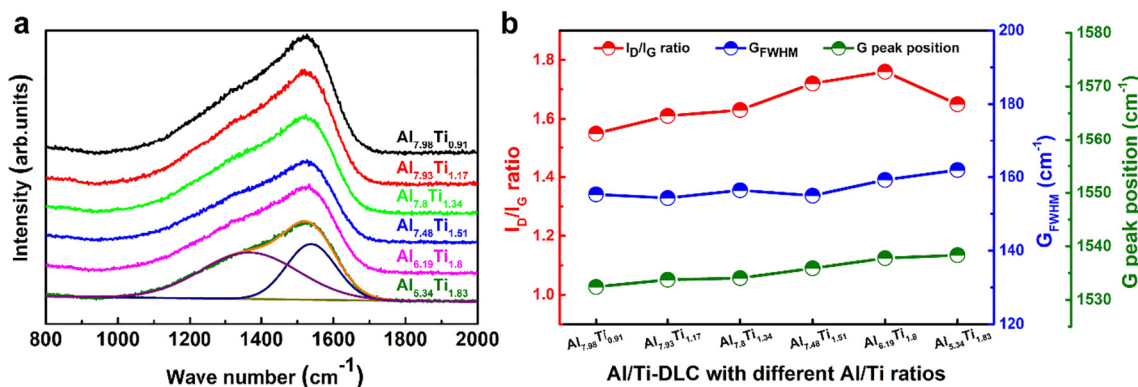
Fig. 5. (a) Raman spectra and (b) corresponding fitted result including I_D/I_G, G_{FWHM}, and G peak position of Al/Ti-DLC films with different Al/Ti ratios.

where *E*, *H*, and *P* are the elastic modulus, hardness, and indentation load of Al/Ti-DLC film, respectively; *b* is 0.016 because of the tetrahedron cone used in this experiment; *c* is the radial crack length; *a* is half length at the diagonal of the indentation. These values inserted in Fig. 6c clearly confirm that the toughness of Al/Ti-DLC film with the Al/Ti ratio (from 8.8 to 3.0) is enhanced. This attributes to the structural graphitization in the films, as shown in Fig. 5b, while the formation of brittle titanium carbide with low fraction almost has no effect on the toughness.

3.4. Roughness

Fig. 7 displays the topographies of Al/Ti-DLC films with different Al/Ti ratios, and the inserted values are the surface roughness, R_a, of Al/Ti-DLC films, which are calculated over 1 μm × 1 μm area. The surface of the DLC film is dense and compact, but the surface morphologies of Al/Ti-DLC films with Al/Ti ratios vary obviously. Following the Al/Ti ratio ranged from 8.8 to 3, the Ra value decreases from 2.81 to 0.36 nm obviously. This largely relies on the combined effect of dispersion and fraction of the formed titanium carbide and aluminum oxide in the films, coinciding with previous result [28]. Previous studies [36–38] reported that that there was almost a linear relationship between the surface roughness and COF and wear rate for DLC films; rough surface was normally accompanied by high friction and wear, because the serious mechanical meshing occurred on the sliding surfaces and the microbumps embedded in each other resulted in the severe wear. Therefore, the R_a values in Fig. 7 suggest that the film with the best tribological properties could be obtained when the Al/Ti ratio is 3.0.

3.5. Tribological properties

The tribological properties of Al/Ti-DLC films are presented in Fig. 8. In the friction curves (Fig. 8a), the COF increases first and then decreases with sliding time during the running-in period for each case;

after that, a stable friction stage is obtained. The average COF values are illustrated in Fig. 8b, which drops significantly from 0.16 to 0.06 with Al/Ti ratio ranged from 8.8 to 3.0. Then, the wear rate is calculated according to Eq. (1), as shown in Fig. 8b. Note that the wear rate of Al/Ti-DLC with Al/Ti ratio also decreases drastically from 10.2×10^{-7} to 4.7×10^{-7} mm^3/Nm, which is affected by the surface roughness of films according to previous reports (Fig. 7) [36–38].

To unveil the underlying mechanism, the SEM micrographs of wear tracks are analyzed first for each case, as given in Fig. 9a. It shows that with decreasing the Al/Ti ratio, the width of wear track becomes narrow; when the Al/Ti ratio decreases to 5.0 from 8.8, the Al/Ti-DLC film is worn through partially and the spalling degree reduces, causing the high wear rate values (Fig. 8b), which is confirmed by the partial enlarged view and internal distribution of the wear track in Fig. S1 and Table S1 of Supporting Information. However, there is no obvious wearing behaviors occurred when the Al/Ti ratio is 3.4 or 3, respectively. This reveals that the major failure mechanism of Al/Ti-DLC film is flaking and breaking, but during the friction process the film is not completely flaked and thus some carbon films still exist at the friction interface, contributing to the friction behavior.

So far, there are three most representative viewpoints for the explanation of the friction mechanism of DLC films, including transfer film theory, sliding interface graphitization theory, and chemical adsorption passivation and dangling bond theory. For the transfer film theory, the DLC film undergoes a phase-structure transformation during the friction process and forms a transfer film with low shear strength at sliding interface, thereby inspiring the low COF. For the sliding interface graphitization theory, the high temperature generated at the sliding interface results in the rupture of C−H bond and thus the hydrogen will be released under the shearing effect, prompting the graphitic transformation from sp^3 to sp^2 hybridization; the graphitic layer between the two contact faces, which has a low shear strength, results in the low-friction behavior. For the dangling bond-passivation theory, most of the hydrogen atoms in the hydrogen-containing DLC films are covalently bound to the carbon. The formation of C−H bond eliminates
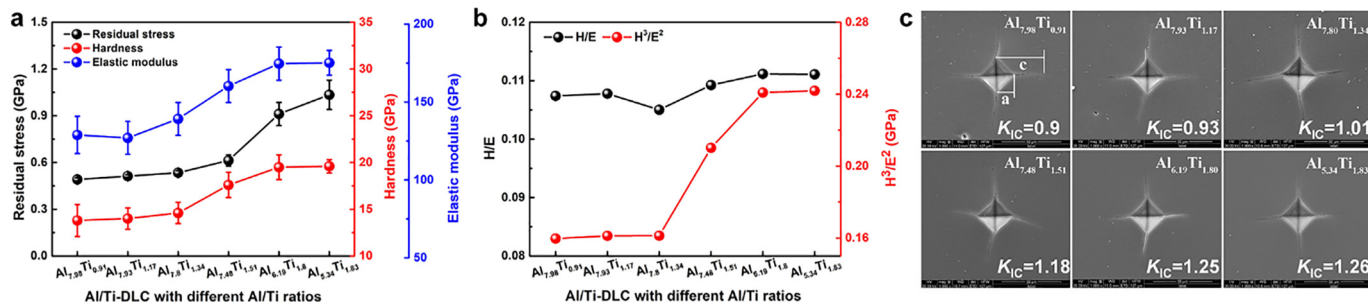

Fig. 6. (a) Residual stress, hardness, elastic modulus, and (b) H/E and H^3/E^2 of Al/Ti-DLC films with different Al/Ti ratios; SEM images of radial cracks at vickers indentation for each case, in which the insets are the fracture toughness values, K_{IC} (units: MPa·m$^{1/2}$).
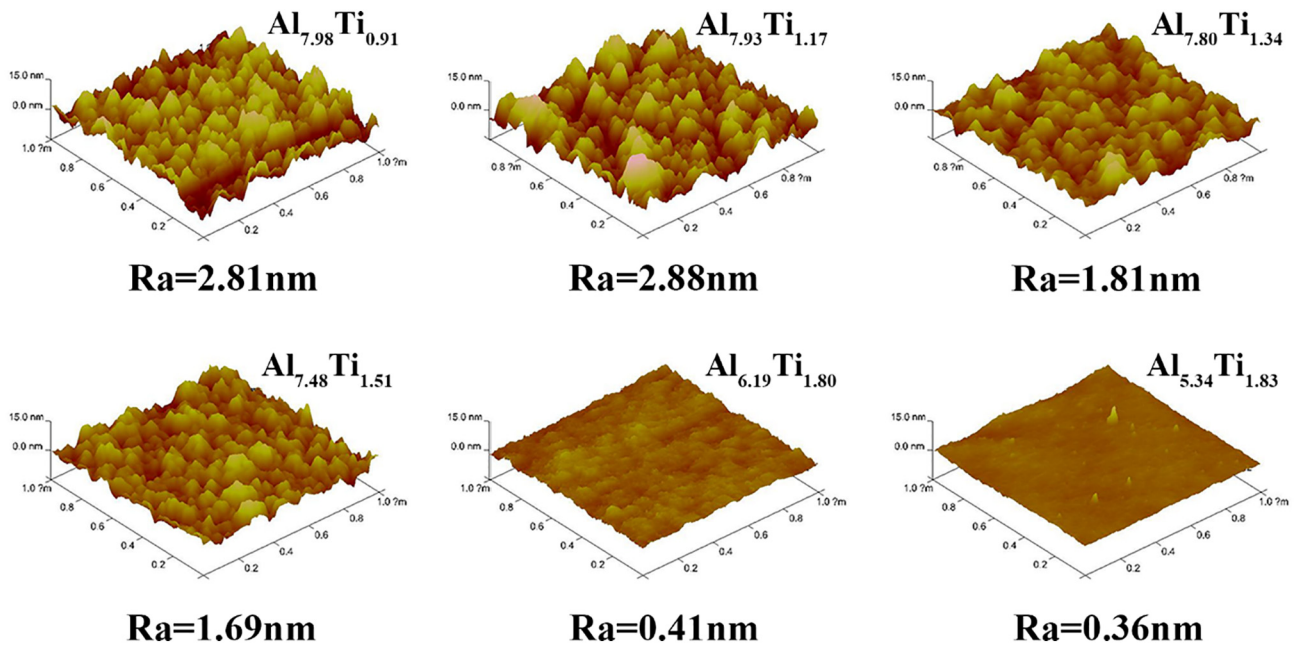
Fig. 7. The tapping mode 3D-AFM surface morphologies of Al/Ti-DLC films as a function of different Al/Ti ratios.

the free σ bond on the surface of the film, while the hydrogen presented in the atomic and molecular state can continuously supplement the hydrogen lost during the friction process due to mechanical wear and thermal desorption, so that the film surface is always in a state maximum passivation, leading to the reduced COF and wear rate.

After friction process, the wear scar from the Si_3N_4 ball is further characterized for each case, which is surrounded by a large amount of abrasive dust (Fig. S2 of Supporting Information) and can be divided into three regions, as shown in Fig. 9b. The region 1 is the surrounding powdery abrasive debris, the region 2 is the lamellar wear debris (Fig. S3 of Supporting Information), and the region 3 is where the Si_3N_4 ball comes into frictional contact with the film directly. Raman spectra of each region proves that the regions 1 and 2 mainly consist of amorphous carbon structures, while the region 3 shows the similar Raman spectra and composition to the Si_3N_4 ball (region 4 in Fig. 9b) without stable transfer film generated. Therefore, on the one hand, it indicates that the transfer film theory is not suitable for explaining the low-friction mechanism of the Al/Ti-DLC film in the present experiment. On the other hand, it is different from with Kong's report [23], in which a thick transfer layer could be formed after sliding against GCr15 steel ball when the co-doped Ti and Al content were 10.06 at.% and 4.78 at. %, respectively. This difference further confirms the strong dependence

of friction behavior of Al/Ti-DLC films on the co-doped metal content, Al/Ti ratio, and mating materials.

Furthermore, Fig. 9c shows the difference in I_D/I_G of wear tracks with different Al/Ti ratios before and after friction process. Compared with the results in intrinsic Al/Ti-DLC films, the I_D/I_G ratio in the wear tracks increases slightly after the friction process when the Al/Ti ratio decreases from 8.8 to 5.0, implying the existence of graphitic process. However, as the Al/Ti ratio further drops to 3.4 and 3.0 from 5.0, the I_D/I_G ratio reduces obviously, suggesting that there is no graphitization occurred. In particular, by further analyzing the change of I_D/I_G ratio and G peak position with sliding time in the $Al_{5.34}Ti_{1.83}$-DLC film, as shown in Fig. 9d, it also confirms that during the running-in (30 s, 1 min, and 3 min) and stable (30 min) friction processes, no graphitic transformation happens, so the graphitization theory also cannot be adopted to explain the friction mechanism of the Al/Ti-DLC films with Al/Ti ratios of 3.4 and 3.0, respectively.

Holmberg et al. [38] reported the frictional contact conditions on different roughness to visually recognize the lubrication and wear failure mechanism of DLC film. For relatively coarse DLC films, the formation of surface graphitization is critical for smooth engineering surfaces; for DLC films with physically smooth surfaces, the ultra-lubricating properties can be explained by hydrogenation of the dangling
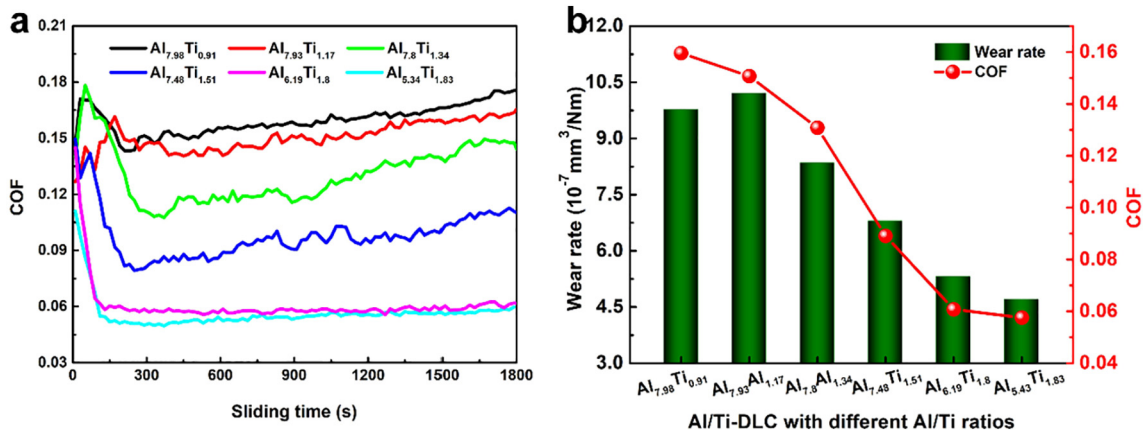

Fig. 8. (a) Friction curves with sliding time and (b) wear rate and COF of Al/Ti-DLC films as a function of Al/Ti ratios.
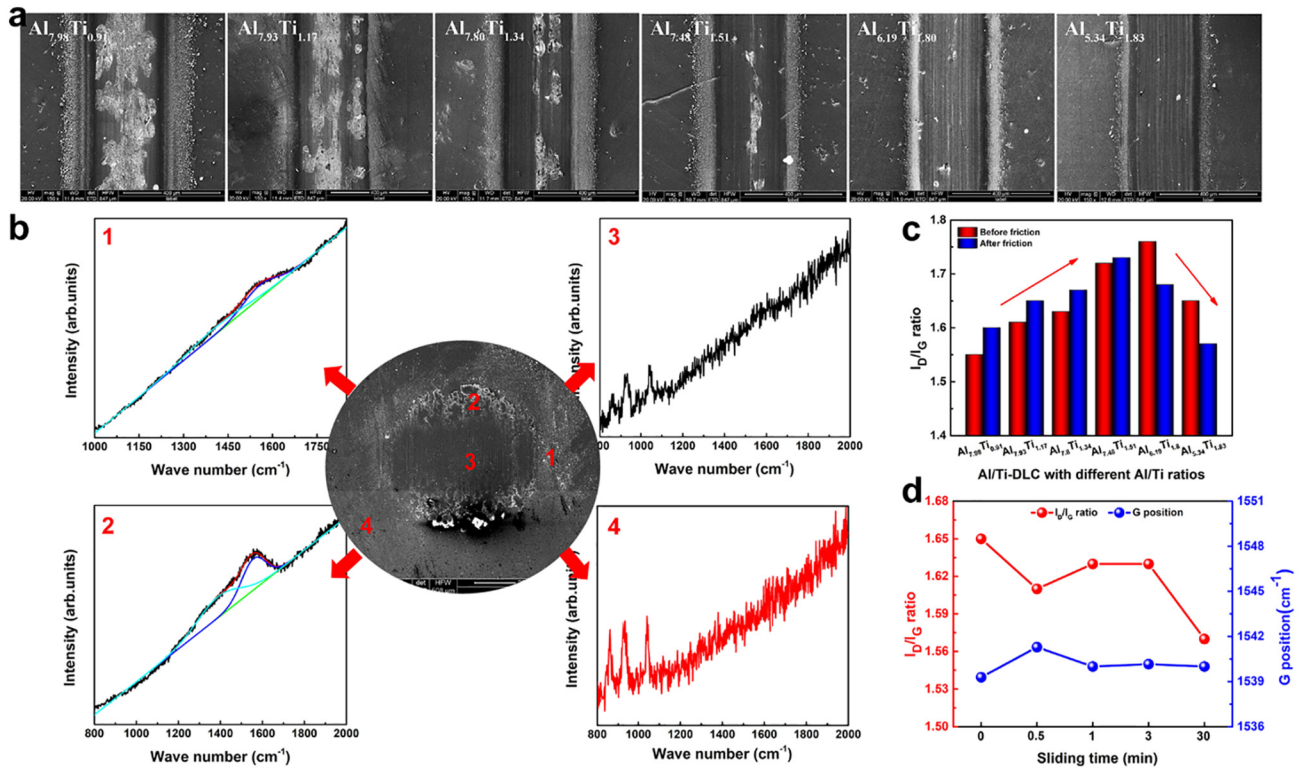
Fig. 9. (a) SEM images of wear tracks of Al/Ti-DLC films with different Al/Ti ratios. (b) Raman diagrams of different regions of wear scar for the $Al_{5.34}Ti_{1.83}$-DLC film. (c) Evolution of I_D/I_G in wear tracks of Al/Ti-DLC films as a function of Al/Ti ratios before and after friction process. (d) Variations of I_D/I_G and G peak position in wear tracks of $Al_{5.34}Ti_{1.83}$-DLC film with different sliding times.
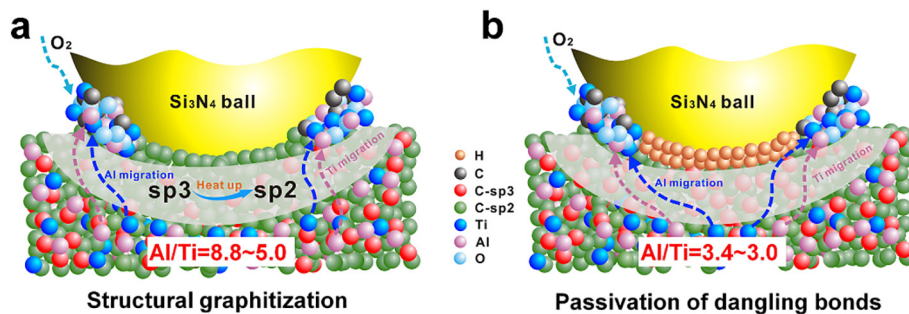

Fig. 10. Schematic representation of friction mechanism of Al/Ti-DLC film against Si_3N_4 ball under the Al/Ti rations of (a) 8.8–5.0 and (b) 3.4–3.0, respectively.

bonds. Therefore, in the present work, when the Al/Ti ratio is 8.8, 6.8, 5.8, or 5.0 separately, the Al/Ti-DLC films has rough surfaces (Fig. 7), and the structural graphitization (Fig. 9c) is also observed, dominating the friction behavior, as shown in Fig. 10a. When the Al/Ti ratio is 3.4 and 3.0, the films show the smooth surface (Fig. 7), and due to the absence of structural graphitization and transfer layer (Fig. 9b and d), the passivation of friction interface caused by H and other gaseous reactive species should be the main mechanism for the low coefficient of friction according to Holmberg's report [38], although it is still difficult to be evaluated due to the limitation of experimental characterization [3], and the corresponding schematic representation of friction mechanism is illustrated in Fig. 10b.

4. Conclusions

Al/Ti-DLC films were prepared by the HIB deposition system. The dependence of microstructure, residual stress, mechanical and tribological poperties of Al/Ti-DLC films on Al/Ti ratios were systematically explored. Results indicated that

(1) The high-throughput preparation of Al/Ti-DLC films with different Al/Ti ratios could be successfully obtained by designing the special Al/Ti composite target, which had the same thickness and total Al/Ti content.

(2) The change of Al/Ti ratios had no effect on the existing states of co-doped Al and Ti in amorphous carbon matrix. The Al existed primarily in the form of oxidized state, while Ti existed mainly as hard titanium carbide and titanium oxide in the as-deposited films. In addition, with the decrease of Al/Ti ratio from 8.8 to 3.0, the graphitization level of Al/Ti-DLC film increased, attributing to the increased content and catalytic effect of Ti atoms.

(3) The residual compressive stress and mechanical property (hardness, elastic modulus, and toughness) of Al/Ti-DLC film were strongly dependent on the Al/Ti ratios, which increased obviously with Al/Ti ratio ranged from 8.8 to 3.0. The increase of residual stress was related with the reduction of Al content and the additional structural distortion caused by titanium carbide. However, the formation and increased fraction of hard titanium carbide contributed to the enhancement of mechanical properties.

(4) The COF and wear rate of Al/Ti-DLC film with decreasing Al/Ti

ratio also drops drastically. When the Al/Ti ratio was 3.0, the minimal COF of 0.06 and wear rate of $4.7 \times 10^{-7} \text{ mm}^3/\text{Nm}$ were obtained. However, due to the difference in Al/Ti ratios, the films exhibited the different friction mechanism. When the Al/Ti ratio changed from 8.8 to 5.0, the structural graphitization was the main friction mechanism. With further decreasing the Al/Ti ratio to 3.4 and 3.0, respectively, the low-friction behavior was primarily governed by the passivation of dangling bonds.

Acknowledgments

Appendix A. Supplementary data

Supplementary data to this article can be found online at https://doi.org/10.1016/j.surfcoat.2019.01.049.

References

[1] J. Vetter, 60 years of DLC coatings: historical highlights and technical review of cathodic arc processes to synthesize various DLC types, and their evolution for industrial applications, Surf. Coat. Technol. 257 (2014) 213–240.

[2] K. Bewilogua, D. Hofmann, History of diamond-like carbon films — from first experiments to worldwide applications, Surf. Coat. Technol. 242 (2014) 214–225.

[3] L. Cui, Z. Lu, L. Wang, Probing the low-friction mechanism of diamond-like carbon by varying of sliding velocity and vacuum pressure, Carbon 66 (2014) 259–266.

[4] R. Bayón, A. Igartua, J.J. González, U. Ruiz de Gopegui, Influence of the carbon content on the corrosion and tribocorrosion performance of Ti-DLC coatings for biomedical alloys, Tribol. Int. 88 (2015) 115–125.

[5] W. Song, Y. Kim, D.S. Jung, S.I. Lee, W. Jung, O.J. Kwon, H.K. Kim, M.S. Kim, K.-S. An, C.-Y. Park, Boron and nitrogen co-doping of diamond-like carbon film for transparent conductive films, Appl. Surf. Sci. 284 (2013) 53–58.

[6] Q. Wang, F. Zhou, Z. Zhou, Y. Yang, C. Yan, C. Wang, W. Zhang, L.K.-Y. Li, I. Bello, S.-T. Lee, Influence of Ti content on the structure and tribological properties of Ti-DLC coatings in water lubrication, Diam. Relat. Mater. 25 (2012) 163–175.

[7] X. Sui, J. Liu, S. Zhang, J. Yang, J. Hao, Microstructure, mechanical and tribological characterization of CrN/DLC/Cr-DLC multilayer coating with improved adhesive wear resistance, Appl. Surf. Sci. 439 (2018) 24–32.

[8] S. Bhowmick, M. Lou, M.Z.U. Khan, A. Banerji, A.T. Alpas, Role of an oxygen atmosphere in high temperature sliding behaviour of W containing diamond-like carbon (W-DLC), Surf. Coat. Technol. 332 (2017) 399–407.

[9] M.H. Ahmed, J.A. Byrne, Effect of surface structure and wettability of DLC and N-DLC thin films on adsorption of glycine, Appl. Surf. Sci. 258 (2012) 5166–5174.

[10] S.I. Hosseini, Z. Javaherian, D. Minai-Tehrani, R. Ghasemi, Z. Ghaempanah, M.A. Firouzjah, B. Shokri, Antibacterial properties of fluorinated diamond-like carbon films deposited by direct and remote plasma, Mater. Lett. 188 (2017) 84–87.

[11] M. Lubwama, B. Corcoran, K.A. McDonnell, D. Dowling, J.B. Kirabira, A. Sebbit, K. Sayers, Flexibility and frictional behaviour of DLC and Si-DLC films deposited on nitrile rubber, Surf. Coat. Technol. 239 (2014) 84–94.

[12] J. Pu, G. Zhang, S. Wan, R. Zhang, Synthesis and characterization of low-friction Al-DLC films with high hardness and low stress, J. Compos. Mater. 49 (2013) 199–207.

[13] N.K. Manninen, F. Ribeiro, A. Escudeiro, T. Polcar, S. Carvalho, A. Cavaleiro, Influence of Ag content on mechanical and tribological behavior of DLC coatings, Surf. Coat. Technol. 232 (2013) 440–446.

[14] H. Cao, F. Qi, X. Ouyang, N. Zhao, Y. Zhou, B. Li, W. Luo, B. Liao, J. Luo, Effect of Ti transition layer thickness on the structure, mechanical and adhesion properties of Ti-DLC coatings on aluminum alloys, Materials 11 (2018), https://doi.org/10.3390/ma11091742.

[15] W. Dai, P. Ke, A. Wang, Microstructure and property evolution of Cr-DLC films with different Cr content deposited by a hybrid beam technique, Vacuum 85 (2011) 792–797.

[16] L. Sun, P. Guo, P. Ke, X. Li, A. Wang, Synergistic effect of Cu/Cr co-doping on the wettability and mechanical properties of diamond-like carbon films, Diam. Relat. Mater. 68 (2016) 1–9.

[17] I.C. Müller, J. Sharp, W.M. Rainforth, P. Hovsepian, A. Ehiasarian, Tribological response and characterization of Mo–W doped DLC coating, Wear 376-377 (2017) 1622–1629.

[18] P.E. Hovsepian, P. Mandal, A.P. Ehiasarian, G. Sáfrán, R. Tietema, D. Doerwald, Friction and wear behaviour of Mo–W doped carbon-based coating during boundary lubricated sliding, Appl. Surf. Sci. 366 (2016) 260–274.

[19] L. Qiang, K. Gao, L. Zhang, J. Wang, B. Zhang, J. Zhang, Further improving the mechanical and tribological properties of low content Ti-doped DLC film by W incorporating, Appl. Surf. Sci. 353 (2015) 522–529.

[20] L. Ji, Y. Wu, H. Li, H. Song, X. Liu, Y. Ye, J. Chen, H. Zhou, L. Liu, The role of trace Ti concentration on the evolution of microstructure and properties of duplex doped Ti(Ag)/DLC films, Vacuum 115 (2015) 23–30.

[21] P. Mandal, A.P. Ehiasarian, P.E. Hovsepian, Tribological behaviour of Mo–W doped carbon-based coating at ambient condition, Tribol. Int. 90 (2015) 135–147.

[22] T. Guo, C. Kong, X. Li, P. Guo, Z. Wang, A. Wang, Microstructure and mechanical properties of Ti/Al co-doped DLC films: dependence on sputtering current, source gas, and substrate bias, Appl. Surf. Sci. 410 (2017) 51–59.

[23] C. Kong, P. Guo, L. Sun, Y. Zhou, Y. Liang, X. Li, P. Ke, K.-R. Lee, A. Wang, Tribological mechanism of diamond-like carbon films induced by Ti/Al co-doping, Surf. Coat. Technol. 342 (2018) 167–177.

[24] X. Li, L. Sun, P. Guo, P. Ke, A. Wang, Structure and residual stress evolution of Ti/Al, Cr/Al or W/Al co-doped amorphous carbon nanocomposite films: insights from ab initio calculations, Mater. Des. 89 (2016) 1123–1129.

[25] X. Li, P. Guo, L. Sun, X. Zuo, D. Zhang, P. Ke, A. Wang, Ti/Al co-doping induced residual stress reduction and bond structure evolution of amorphous carbon films: An experimental and ab initio study, Carbon 111 (2017) 467–475.

[26] S. Zhou, L. Ma, L. Wang, Q. Xue, Tribo-pair dependence of friction and wear moisture sensitivity for a-C:Si:Al carbon-based coating, J. Non-Cryst. Solids 358 (2012) 3012–3018.

[27] X. Liu, J. Hao, J. Yang, J. Zheng, Y. Liang, W. Liu, Preparation of superior lubricious amorphous carbon films co-doped by silicon and aluminum, J. Appl. Phys. 110 (2011) 053507.

[28] X. Pang, L. Shi, P. Wang, Y. Xia, W. Liu, Effects of Al incorporation on the mechanical and tribological properties of Ti-doped a-C:H films deposited by magnetron sputtering, Curr. Appl. Phys. 11 (2011) 771–775.

[29] Y. Wu, S. Zhou, W. Zhao, L. Ouyang, Comparative corrosion resistance properties between (Cu, Ce)-DLC and Ti co-doped (Cu, Ce)/Ti-DLC films prepared via magnetron sputtering method, Chem. Phys. Lett. 705 (2018) 50–58.

[30] W. Dai, J. Liu, D. Geng, P. Guo, J. Zheng, Q. Wang, Microstructure and property of diamond-like carbon films with Al and Cr co-doping deposited using a hybrid beams system, Appl. Surf. Sci. 388 (2016) 503–509.

[31] W. Dai, A. Wang, Deposition and properties of Al-containing diamond-like carbon films by a hybrid ion beam sources, J. Alloys Compd. 509 (2011) 4626–4631.

[32] W. Dai, H. Zheng, G. Wu, A. Wang, Effect of bias voltage on growth property of Cr-DLC film prepared by linear ion beam deposition techniqu, Vacuum 85 (2010) 231–235.

[33] A.C. Ferrari, Determination of bonding in diamond-like carbon by Raman spectroscopy, Diam. Relat. Mater. 11 (2002) 1053–1061.

[34] X. Li, L. Li, D. Zhang, A. Wang, Ab initio study of interfacial structure transformation of amorphous carbon catalyzed by Ti, Cr, and W transition layers, ACS Appl. Mater. Interfaces 9 (2017) 41115–41119.

[35] W. Dai, P. Ke, M. Moon, K.R. Lee, A. Wang, Investigation of the microstructure, mechanical properties and tribological behaviors of Ti-containing diamond like carbon films fabricated by a hybrid ion beam method, Thin Solid Films 520 (2012) 6057–6063.

[36] A.B. Vladimirov, I.S. Trakhtenberg, A.P. Rubshtein, S.A. Plotnikov, O.M. Bakunin, L.G. Korshunov, E.V. Kuzmina, The effect of substrate and DLC morphology on the tribological properties coating, Diam. Relat. Mater. 9 (2000) 838–842.

[37] K.P. Shaha, Y.T. Pei, D. Martinez-Martinez, J.T.M. De Hosson, Influence of hardness and roughness on the tribological performance of TiC/a-C nanocomposite coatings, Surf. Coat. Technol. 205 (2010) 2624–2632.

[38] K. Holmberg, H. Ronkainen, A. Laukkanen, K. Wallin, Friction and wear of coated surfaces — scales, modelling and simulation of tribomechanisms, Surf. Coat. Technol. 202 (2007) 1034–1049.